NASA TECHNICAL NOTE

NASA TN D-5887

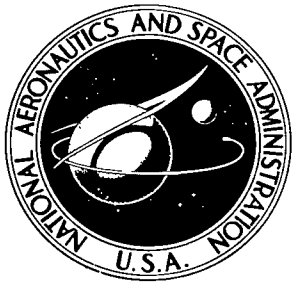

NASA TN D-5887
c. 1

HEAT TRANSFER IN A 60° HALF-ANGLE OF CONVERGENCE NOZZLE WITH VARIOUS DEGREES OF ROUGHNESS

by Meyer Reshotko, Donald R. Boldman, and Robert C. Ehlers

Lewis Research Center
Cleveland, Ohio 44135

NATIONAL AERONAUTICS AND SPACE ADMINISTRATION • WASHINGTON, D. C. • JULY 1970

1. Report No. NASA TN D-5887	2. Government Accession No.	3. Recipient's Catalog No.
4. Title and Subtitle HEAT TRANSFER IN A 60° HALF-ANGLE OF CONVERGENCE NOZZLE WITH VARIOUS DEGREES OF ROUGHNESS		5. Report Date July 1970 6. Performing Organization Code
7. Author(s) Meyer Reshotko, Donald R. Boldman, and Robert C. Ehlers		8. Performing Organization Report No. E-5597
9. Performing Organization Name and Address Lewis Research Center National Aeronautics and Space Administration Cleveland, Ohio 44135		10. Work Unit No. 129-01 11. Contract or Grant No. 13. Type of Report and Period Covered Technical Note
12. Sponsoring Agency Name and Address National Aeronautics and Space Administration Washington, D.C. 20546		14. Sponsoring Agency Code

15. Supplementary Notes

16. Abstract

An experimental heat-transfer study has been conducted in a converging-diverging nozzle having various values of wall roughness. The working fluid was air, which was heated to a stagnation temperature of 970° R (538 K). The stagnation pressure was varied from 30 to 300 psia (20.7 to 206.9 N/cm^2). The nozzle was roughened by a sandblasting technique to three levels of roughness: 120, 175, and 325 rms (305×10^{-6}, 445×10^{-6}, and 826×10^{-6} cm rms). Both a cooled and an adiabatic inlet, each having smooth walls, were used to determine the effects of the thermal history of the fluid on the nozzle heat transfer.

17. Key Words (Suggested by Author(s)) Heat transfer Nozzles Roughness	18. Distribution Statement Unclassified - unlimited		
19. Security Classif. (of this report) Unclassified	20. Security Classif. (of this page) Unclassified	21. No. of Pages 30	22. Price* $3.00

*For sale by the Clearinghouse for Federal Scientific and Technical Information Springfield, Virginia 22151

HEAT TRANSFER IN A 60° HALF-ANGLE OF CONVERGENCE NOZZLE WITH VARIOUS DEGREES OF ROUGHNESS

by Meyer Reshotko, Donald R. Boldman, and Robert C. Ehlers
Lewis Research Center

SUMMARY

An experimental study was conducted to determine the effects of various degrees of surface roughness on heat transfer in a converging-diverging nozzle. The 60^{o}-15^{o} half-angle nozzle was roughened by a sandblasting technique to three levels of roughness: 120, 175, and 325 rms (305×10^{-6}, 445×10^{-6}, and 826×10^{-6} cm rms). At each roughness level nearly an order of magnitude range in Reynolds number was obtained by varying the stagnation pressure from 30 to 300 psia (20.7 to 206.9 N/cm^2). The Reynolds number range at the throat station varied from 6×10^5 to 5×10^6. However, the stagnation temperature was always the same at a nominal value of 970^{o} R (538 K). These operating conditions made it possible to obtain heat transfer in the turbulent, transition, and laminarization regimes.

The results show the following:

(1) Roughness causes transition from laminarized flow to take place at a lower Reynolds number than that for a smooth wall.

(2) In the laminarization regime, heat transfer is unaffected by roughness.

(3) In the turbulent regime, the heat transfer is not noticeably affected by roughness until the roughness height is in the region of or greater than the approximated sublayer height.

(4) An adiabatic inlet causes greater nozzle heat transfer than a cooled inlet for all values of roughness.

INTRODUCTION

In a rocket nozzle it is desirable to minimize the propellant-gas to nozzle-wall heat transfer to obtain high thrust efficiency. The results of rather extensive studies of gas to wall heat transfer in a smooth wall rocket-type nozzle have been presented in refer-

ences 1 to 4. However, in these references little consideration was given to the effects of the wall surface finish on the nozzle heat transfer. The purpose of this report is to experimentally determine the effects of various degrees of surface roughness on the heat transfer in a rocket-type nozzle.

In the majority of present day chemical rockets, the nozzle surface finish is somewhat rougher than that of the smooth wall nozzles of references 1 to 4. Furthermore, after long periods of operation at high temperatures the walls of most nozzles become rougher due to erosion and oxidation. These differences in surface finish introduce questions concerning the applicability of the smooth wall heat-transfer results to a rocket nozzle. Another source of roughness in certain rocket nozzles is a ceramic coating which provides insulation between the hot propellant gas and the cooled wall. A knowledge of the effects of roughness on the heat transfer is necessary to determine whether the reduction due to the insulation is offset by an increase in heat transfer resulting from the rougher surface. In all of these cases acceleration causes a thinning of the boundary layer whereas roughness causes an increase in the surface height.

In order to obtain an understanding of the heat-transfer effects of roughness in accelerated flow, one can first consider independently the behavior of heat transfer in nozzles (accelerated flow) with smooth walls, and heat transfer in pipes (nonaccelerated flow) with rough walls. The heat-transfer studies of references 1 to 4 have shown that the heat transfer in accelerated flow differs considerably from that predicted by unaccelerated flow theory and experiment. In accelerated flow there are two distinct regimes of heat-transfer rate that are both less than that of conventional turbulent pipe flow. The high Reynolds number regime represents turbulent heat transfer for accelerated flows and the low Reynolds number regime suggests a laminarization phenomenon. The laminarization depends on the flow acceleration and is further discussed in reference 5.

A great deal of work has been done studying the effects of roughness on heat transfer in unaccelerated flow, mainly pipe flow. The surfaces were roughened for either one of two reasons: (1) to simulate a naturally rough surface, or (2) to enhance the heat transfer between the fluid and pipe wall. All of the experimental investigators (refs. 6 to 9) found that increased wall roughness increased the heat transfer, in one case by a factor of three. However, in all cases there was a corresponding increase in pressure drop such that the benefit of increased heat transfer was overshadowed by the penalty in pressure drop. Various types of surface roughness configurations were used on the inner pipe walls. One of the first to artificially roughen a pipe was Nikuradse (ref. 10) who glued sand to the inside of the pipe. Cope (ref. 6) used an internally knurled pipe, Sams (ref. 7) used circular tubes having internal square threads, and Nunner (ref. 9) obtained his roughness by using springy split ring tubes set apart at equal distances inside the pipe. Although this is only a partial list of the investigators it covers a wide variety of the roughness configurations.

This report is an experimental study of the effects of various degrees of surface

roughness on heat transfer in a converging-diverging nozzle. Air at a stagnation temperature of 970° R (538 K) was used as the working fluid. The pressure was varied from 30 to 300 psia (20.7 to 206.9 N/cm^2) yielding an order of magnitude range in Reynolds number at each station. The Reynolds number range at the throat station was 6×10^5 to 5×10^6. The 60°-15° half-angle nozzle was roughened by a sandblasting technique to three levels of roughness: 120, 175, and 325 rms (305×10^{-6}, 445×10^{-6}, and 826×10^{-6} cm rms). Both a cooled and an adiabatic inlet each having smooth walls were used to determine the effects of the thermal history of the fluid on the nozzle heat transfer.

SYMBOLS

A	cross-sectional area
C_1, C_2, C_3	constants
C_f	skin friction
D	local diameter
e	roughness height
g_c	gravitational constant
h	heat-transfer coefficient
i	enthalpy
p	pressure
Pr	Prandtl number
q	local heat flux
Re	Reynolds number
T	total temperature
t	static temperature
u	velocity in axial direction
u*	shear velocity, $\sqrt{(\tau_w/\rho_w)g_c}$
u^+	nondimensional velocity, u/u*
x	axial coordinate measured from nozzle throat
Y	distance along heat-flux meter measured from gas-side wall
y	distance normal to the wall

y^+ nondimensional distance normal to the wall

β angular position of nozzle instrumentation

Δ thickness of thermal boundary layer

μ dynamic viscosity

ρ gas density

τ shear stress

φ energy thickness of boundary layer

Subscripts:

ad adiabatic wall condition

D based on diameter

e evaluated at edge of boundary layer

i based on enthalpy

m heat flux meter

ref reference condition

s static condition

t throat

w wall condition

φ based on energy thickness

0 stagnation condition

∞ free-stream condition

APPARATUS

The experimental apparatus, shown in figure 1, comprised a heat exchanger, diffuser, plenum, cylindrical inlet, test nozzle, and exhaust system. Uncooled- (adiabatic-wall) and cooled-wall pipe inlets having inside diameters of 6.5 inches (16.5 cm) were coupled to a 60° half-angle of convergence by 15° half-angle of divergence (60°-15° converging-diverging) water-cooled nozzle. These inlets will hereinafter be referred to as simply the adiabatic or cooled inlets, respectively.

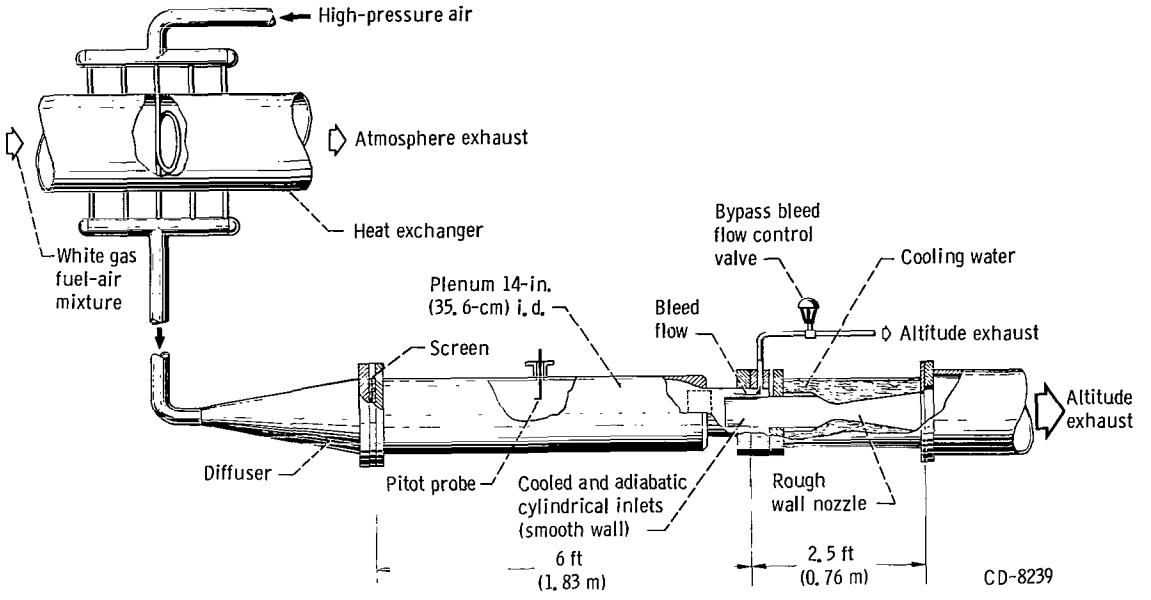

Figure 1. - Schematic diagram of nozzle heat-transfer facility.

Inlets

The adiabatic and cooled inlets had total lengths of 17.0 and 37.6 inches (43.2 and 95.5 cm), respectively. The plenum boundary layer bleed flow was adjusted to initiate the velocity boundary layer at this leading edge of the inlets. The thermal boundary layer developed over a length of 24.2 inches (61.5 cm) in the cooled inlet. In tests with the adiabatic inlet the thermal layer started to develop at the nozzle entrance. Details concerning the materials and fabrication of the adiabatic and cooled inlets can be obtained from references 2 and 5, respectively.

Nozzle

The water-cooled nozzle is shown in figure 2. This nozzle had a nominal throat diameter and radius of curvature of 1.5 inches (3.8 cm). The nozzle had a contraction area ratio of 18.8 and expansion area ratio of 3.3 (Mach 2.7). The nozzle was machined from an AISI 304 stainless steel forged billet. Water was directed over the outside of the 0.5 inch (1.27 cm) thick wall by means of Lucite shrouds.

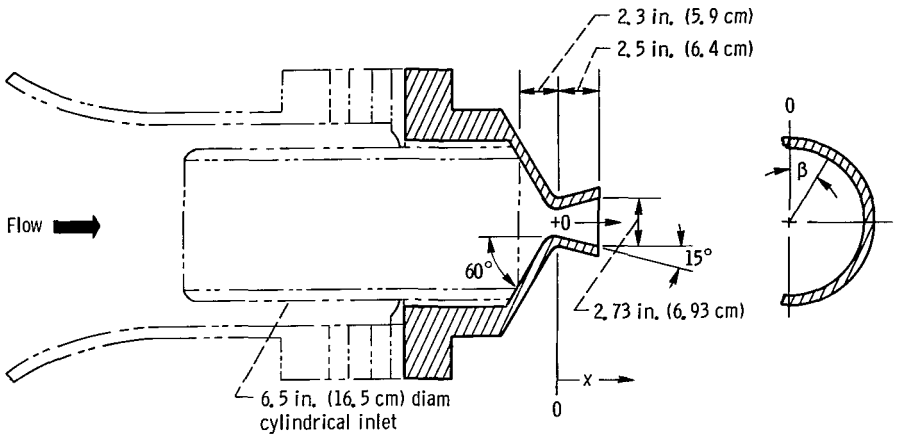

Station	Area ratio, A/A_t	Angular position, β, deg		Axial distance, x		Diameter, D	
		Pressure tap	Heat-flux meter	in.	cm	in.	cm
2	14.663	180	0	-2.085	-5.296	5.740	14.580
3	9.352	77	257	-1.752	-4.450	4.584	11.643
4	7.769	129	309	-1.635	-4.153	4.178	10.612
5	6.299	180	0	-1.515	-3.848	3.762	9.555
6	3.322	231	51	-1.206	-3.063	2.732	6.939
7	2.373	283	103	-1.020	-2.591	2.309	5.865
8	1.341	334	154	-.581	-1.476	1.736	4.409
9	1.023	26	206	-.146	-.371	1.516	3.851
10	1.000	77	257	0	0	1.499	3.807
11	1.030	129	309	.150	.381	1.521	3.863
12	1.090	180	0	.277	.704	1.565	3.975
13	1.172	231	51	.400	1.016	1.623	4.122
14	1.349	283	103	.622	1.580	1.741	4.422
15	1.876	334	154	1.209	3.071	2.053	5.215

Figure 2. - Instrumentation for 60°-15° nozzle.

INSTRUMENTATION

Local heat-transfer rates and wall static pressures were measured at stations 2 to 15 in the nozzle as noted in figure 2. Nozzle wall temperatures were calculated at these stations.

Static Pressures

Nozzle wall static pressure taps having a diameter of 0.031 inch (0.079 cm) were coupled to manometers containing mercury and dibutyl phthalate. These particular fluids were selected to provide good sensitivity throughout the entire Mach number range of the nozzle. Manometer reference pressures were measured with Bourdon tube gages.

Fluid temperature corrections were applied in the reduction of the manometer data. The ratios of static to total pressure at each station have been presented for smooth wall tests in reference 2. These pressure ratios are also applicable to the present study in which the wall of the nozzle was artificially roughened.

Heat-Flux Meter

Steady-state measurements of the gas-side wall temperature and local heat-transfer rates were obtained by means of an Inconel plug-type heat-flux meter shown in figure 3.

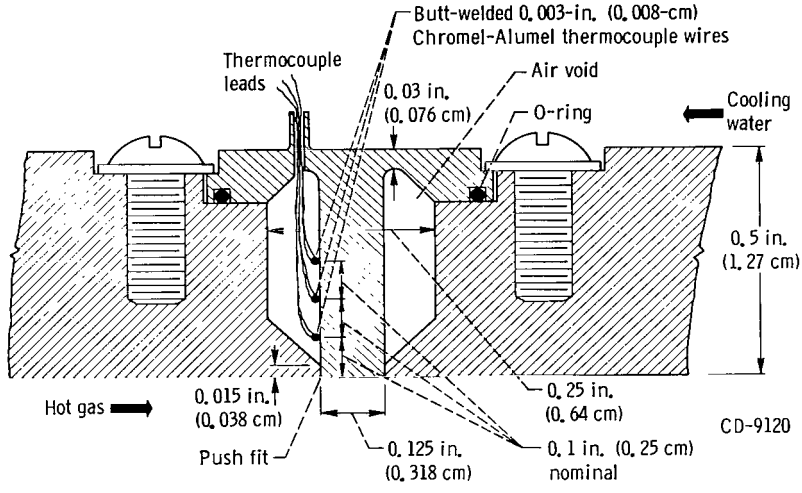

Figure 3. - Inconel heat-flux meter.

Three Chromel-Alumel 0.003-inch (0.008-cm) wire thermocouples were spot-welded to the 0.125-inch diameter (0.318-cm-diam.) Inconel plug. The nominal thermocouple spacing of 0.1 inch (0.25 cm) was determined to the nearest 0.001 inch (0.003 cm) by a microscope. The meters were installed with a push fit at the gas side of the nozzle and were sealed at the water-cooled side by means of an 0-ring. The air column surrounding the plug provided the thermal insulation necessary for one-dimensional heat conduction through the shaft. Each heat-flux meter was located 180^{o} from the static pressure tap at a given station. The relative orientation of the heat meters and pressure taps are given in the table in figure 2.

METHOD OF ROUGHENING

Neither the type of rough surface used by other investigators or the methods used to obtain them were available to us in the study of nozzle roughness effects on heat transfer. The gluing of sand to the surface as was done in reference 10 was suitable for velocity profile measurements. However, for heat-transfer surveys sand is a very poor material since its thermal properties are vastly different from those of the nozzle wall. Useful heat-transfer results can be obtained only when the nozzle wall is homogeneous in material. Internal square threads, as used by the author of reference 7 and many others, have the advantage of clearly defined roughness dimensions. Adjusting the width and depth of cut defines quantitatively the roughness height and pitch. However, for the purposes of this report, this type of roughness is unacceptable. We are interested in a "natural" type of roughness where the peaks and valleys are connected by a gradual slope rather than a vertical face. Second, it would be very difficult to machine the nozzle, and third it would ruin all the instrumentation that is built into the nozzle wall.

The nozzle wall roughnesses used in this study were obtained by a sand or grit blasting technique. This method left a naturally rough surface with minimal damage to the instrumentation. The range of roughness levels was obtained by varying the size and material of the abrasive and the blasting pressure. The most uniform roughening of the entire nozzle surface is obtained when the sandblasting nozzle is perpendicular to the surface being roughened. However, because of the relatively large size of the blasting nozzle and the convergence and divergence angles of the test nozzle this was not easily attained. Figure 4(a) shows the converging section of the 60° nozzle with a smooth surface. Figure 4(b) is a closeup of the same nozzle after it has been roughened to 120 rms (305×10^{-6} cm rms).

The roughened surface was measured with a roughness meter giving a root mean square value of surface height. The roughness cutoff width was 0.030 inch (0.762 mm). The range of roughness in the nozzle was within ±10 percent of the nominal value.

DATA REDUCTION

The local heat flux q was computed from the observed temperature gradient in the heat-flux meters. This temperature gradient is described by the Fourier conduction equation which can be integrated to yield

$$-qY = C_1 t_m^2 + C_2 t_m + C_3$$

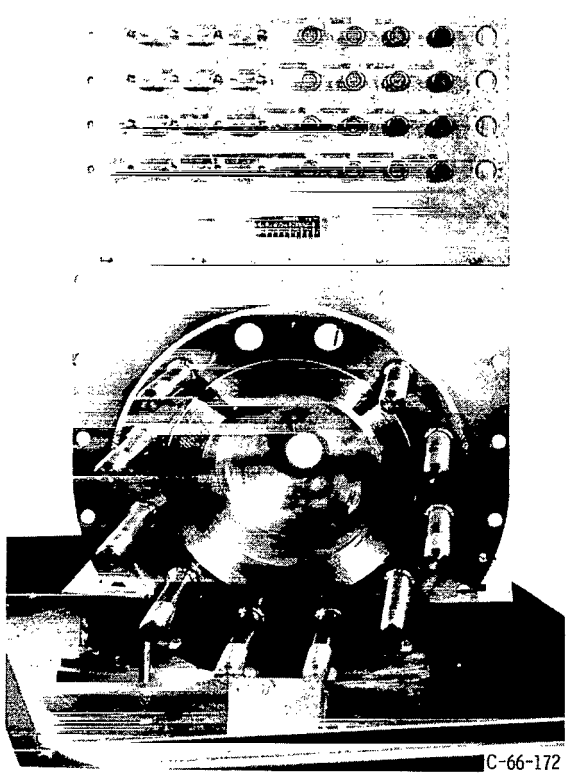

(a) Smooth surface.

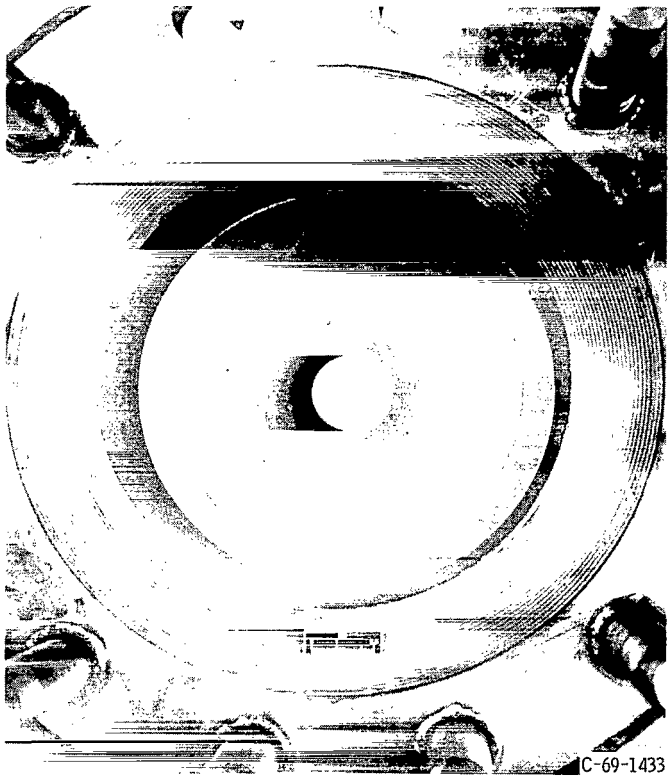

(b) Surface roughness, 120 rms (305×10^{-6} cm rms).

Figure 4. - Converging section of a 60° half-angle of convergence nozzle.

The constants C_1 and C_2 were determined from a thermal-conductivity calibration of the Inconel specimen which was used to fabricate the heat-flux meters. The values of C_1 and C_2 are given in reference 2. The unknowns q and C_3 were determined from the simultaneous solution of two equations containing the measured temperature t_m and the corresponding thermocouple location Y at two of the three measuring stations on the heat-flux meter. The wall temperature was computed by setting $Y = 0$.

The heat-flux error considerations discussed in references 2 and 5 are also applicable to the present study. The principal error in the measured heat flux is associated with the air gap surrounding the heat-flux meter. This air gap effect tends to increase the measured heat flux through local distortion of the wall temperature distribution (ref. 11). However, in reference 5 it was concluded that corrections to the one-dimensional heat-flux measurements were unnecessary. The error in heat flux is expected to be within 10 percent of the measured value.

The nozzle heat transfer is presented in terms of the heat-transfer coefficient h_i as well as the nondimensional parameter $St_{ref}Pr^{0.7}$. The distributions of the heat-transfer coefficient are presented as functions of the axial distance x, whereas the $St_{ref}Pr^{0.7}$

grouping is given as a function of Reynolds number based on local diameter $Re_{D, ref}$.

The heat-transfer coefficient is given by

$$h_i = \frac{q}{i_{ad} - i_w}$$

where the adiabatic enthalpy was calculated from

$$i_{ad} = i_s + Pr^{1/3}(i_0 - i_s)$$

The nondimensional heat-transfer grouping $St_{ref}Pr^{0.7}$ is given by

$$St_{ref}Pr^{0.7} = \frac{h_i}{\rho_{ref} u_\infty} Pr^{0.7}$$

The Reynolds number based on the local diameter $Re_{D, ref}$ is given by

$$Re_{D, ref} = \frac{\rho_{ref} u_\infty D}{\mu_{ref}}$$

A Prandtl number of 0.71 was assumed in the previous equations. The subscript ref denotes that properties were evaluated at a reference enthalpy condition given by

$$i_{ref} = i_s + 0.5(i_w - i_s) + 0.22\ Pr^{1/3}(i_0 - i_s)$$

PROCEDURE

Tests were conducted at stagnation pressures ranging from about 30 to 300 psia (20.7 to 207 N/cm^2). The stagnation temperature for all tests was nominally 970^o R (538 K). The tests were duplicated at each value of wall roughness to ensure repeatability of the results. All temperature data were recorded four times by an automatic voltage digitizer and paper tape system in order to confirm steady-state operation and allow for the averaging of small recording errors. Final data processing was achieved by means of a digital computer.

RESULTS AND DISCUSSION

The heat-transfer results are presented graphically in both a nondimensional and a dimensional manner. The nondimensional form of the heat transfer is given by the Stanton-Prandtl number grouping $St\text{-}Pr^{0.7}$, whereas the dimensional form of the heat transfer is presented in terms of a heat-transfer coefficient h_i.

The plenum pressure is varied in order to get different flow rates which in turn give a range of Reynolds numbers at each station. The heat transfer ($St\text{-}Pr^{0.7}$) at each station is presented as a function of Reynolds number with the nozzle roughness acting as a parameter. In order to show the effects of the thermal history of the fluid prior to entering the nozzle, the heat transfer is presented for tests with both adiabatic and cooled inlets. The advantage of this particular nondimensional presentation is that it shows the laminarized and turbulent modes of heat transfer as distinct regions which can be identified by a Reynolds number in which the reference dimension is the diameter. The diameter is chosen as a convenient dimension since it is approximately proportional to the boundary layer thickness which, of course, would be a more appropriate dimension if it were known (e.g., see ref. 3). Therefore, it must be remembered that two points at the same Reynolds number based on diameter, but at different stations, do not necessarily have the same heat transfer.

The heat-transfer coefficient h_i is presented as a function of axial distance from the nozzle throat for a given plenum pressure with the nozzle roughness as a parameter. This presentation shows the direct magnitude change in heat-transfer coefficient and its axial distribution, which is not clear from the $St\text{-}Pr^{0.7}$ against $Re_{D,ref}$ portrayal.

Stanton-Prandtl Grouping of Heat Transfer

The variation of $St\text{-}Pr^{0.7}$ at stations 4, 8, 10, and 13 is shown since they represent significant locations in the subsonic, sonic, and supersonic regimes of flow. Information on nozzle station location is found in figure 2. Before presenting the effects of roughness on heat transfer in accelerated flow it is worthwhile to review the effects of flow acceleration on heat transfer for a smooth surface.

Heat transfer in a smooth nozzle. - Figure 5(a) shows the experimental heat-transfer parameter with respect to Reynolds number for a smooth nozzle surface at stations 4, 8, 10, and 13 with a cooled pipe inlet. It also shows the standard pipe-flow type of nozzle correlations and an integral method for predicting heat transfer. The results for stations 4, 8, and 10 have been presented in reference 5; however, the results for station 13 are being presented here for the first time.

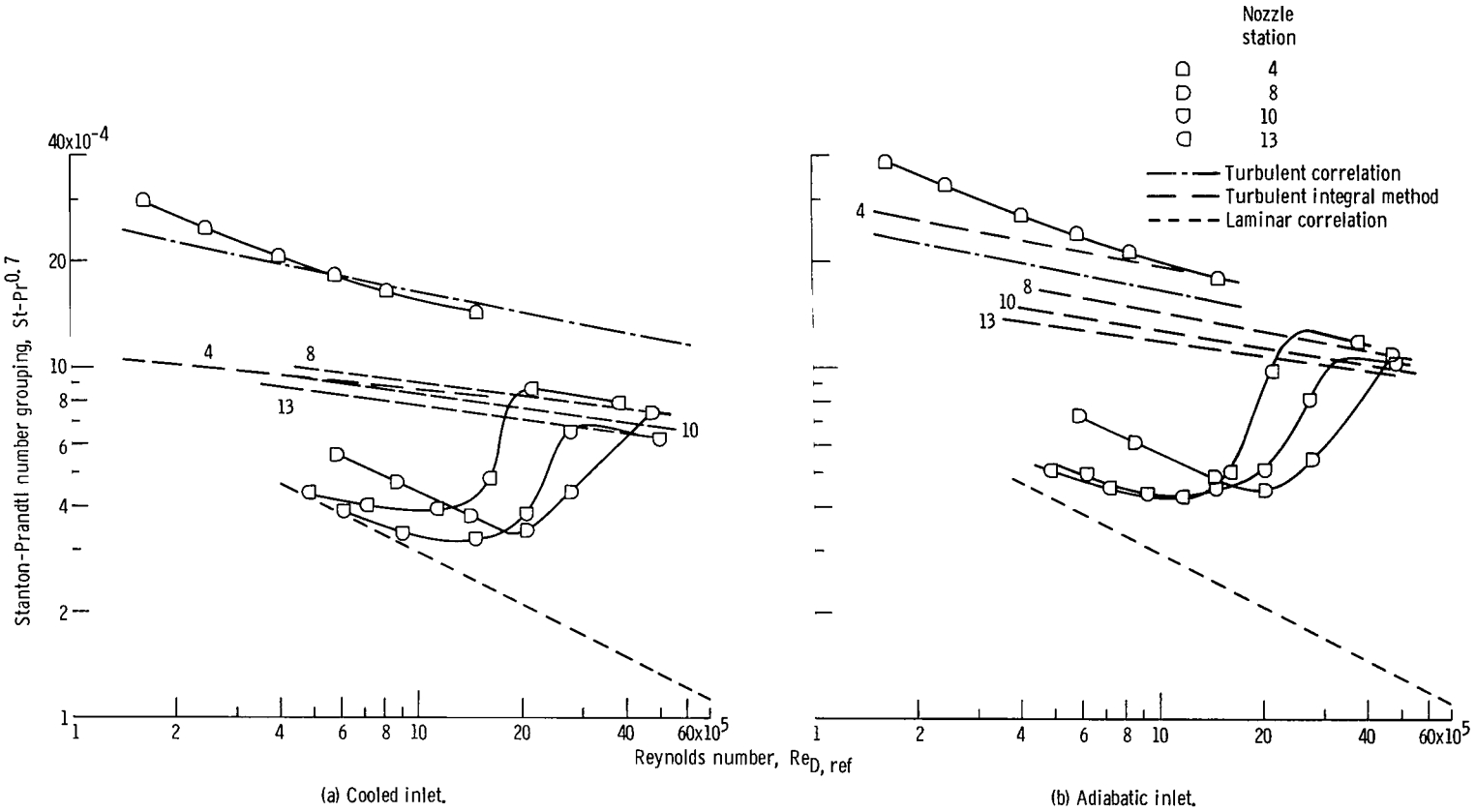

(a) Cooled inlet.

(b) Adiabatic inlet.

Figure 5. - Stanton Prandtl number grouping as function of Reynolds number at various stations in smooth nozzle.

The turbulent correlation

$$St_{ref} Pr^{0.7} = 0.026\ Re_{D,ref}^{-0.2}$$

and the laminar correlation

$$St_{ref} Pr^{0.7} = 0.29\ Re_{D,ref}^{-0.5}$$

frame the results very well. Although there now are much better methods of predicting nozzle heat transfer, these correlations represent the upper and lower limits of the experimental results and will serve as reference levels. However, they show no comprehension of acceleration or fluid thermal history.

Predictions based on the integral boundary layer analysis of reference 12, as illustrated by the straight dashed lines of figure 5, represent a considerable improvement over the results based on the previously mentioned correlations. In this method the heat transfer is related to an energy thickness φ, where

$$\varphi = \int_0^{\Delta} \frac{\rho u}{\rho_e u_e} \left(1 - \frac{T - T_w}{T_0 - T_w}\right) dy$$

The Stanton number is expressed as

$$St = \frac{\frac{C_f}{2}(R_\varphi)}{1 - 5\left[\frac{C_f}{2}(R_\varphi)\right]^{1/2}\left[1 - Pr + \ln\left(\frac{6}{5\ Pr + 1}\right)\right]}$$

This method which takes acceleration and thermal history into account predicts the turbulent heat transfer very well near the throat (ref. 5).

Station 4 (fig. 5) is in the subsonic region just downstream of the nozzle inlet. The Mach number at this station is 0.05 based on the measured static pressure in conjunction with isentropic flow theory. The heat-transfer parameter corresponds very closely to that of the turbulent flow correlation. Although acceleration has started at the nozzle inlet, the resulting heat transfer has not been significantly affected. Heat transfer is strongly dependent on previous fluid history and in this case the fluid has a long history of turbulent flow in the inlet pipe and the change in heat-transfer rate lags the increase in fluid velocity. The effects of acceleration on the nozzle heat transfer are more fully

pronounced at station 8. This station is located in the subsonic region just upstream of the throat. The heat-transfer parameter for the highest Reynolds number corresponds to a turbulent boundary layer (ref. 5). As the Reynolds number decreases, $St\text{-}Pr^{0.7}$ decreases sharply until $Re_{D,ref} = 2\times10^6$, after which it increases for decreasing Reynolds number. Moving downstream to the geometric throat, the results at station 10 show much the same trends as were noted at station 8; however, there is one more data point in the high heat-transfer regime corresponding to a turbulent boundary layer.

When using the coordinates of $St\text{-}Pr^{0.7}$ against $Re_{D,ref}$, two separate regimes of heat transfer emerge with a third regime connecting the two. This was also observed by the authors of references 3 to 5. The mode of heat transfer in the upper regime is turbulent. In the lower regime the heat transfer reflects a reduction in turbulence commonly called laminarization. Although the heat transfer may be close to the values based on the correlation for a laminar boundary layer, there is reason to believe the structure of the thermal boundary layer remains turbulent for the total plenum pressures used in this report (ref. 5). The term laminarization may not be an appropriate description of this phenomenon, but since it is used frequently in the literature it is used in this report to mean reduced turbulence. The heat-transfer regime connecting the upper and lower regimes obviously corresponds to a transition phenomenon.

The effect of acceleration on the heat-transfer results at the supersonic station (station 13) is similar to that observed in the throat region (station 8 and 10). The best way to compare the stations to each other is to start at the nozzle entrance and move downstream in the nozzle. At station 4 the heat-transfer parameters are all in the turbulent mode. Downstream at station 8 where the acceleration is a maximum the heat-transfer mode is turbulent at the high Reynolds number and goes through transition to laminarization as $Re_{D,ref}$ decreases. At station 10, as the flow acceleration decreases, there are fewer points in the laminarization regime and more in the turbulent. Transition to the turbulent regime occurs at a lower Reynolds number than at station 8. At station 13, a further decrease in acceleration rate causes the turbulent heat-transfer parameter to increase and further reduces the Reynolds number at which transition takes place.

In figure 5(b) the heat-transfer results for the adiabatic inlet are presented. They are similar to those of the cooled inlet except that for a given Reynolds number the corresponding value of $St\text{-}Pr^{0.7}$ is higher. The increase in $St\text{-}Pr^{0.7}$ is 50 and 25 percent for the turbulent and laminarized regimes, respectively. With the cooled inlet the thermal boundary layer begins to grow in the inlet and continues growing in the nozzle. With the adiabatic inlet the thermal boundary layer does not exist in the inlet and starts growing at the entrance of the nozzle. This means that at all locations in the nozzle the thermal boundary layer produced using the cooled inlet is thicker than that using the adiabatic inlet. Since the thermal boundary layer acts as an insulator, the heat transfer decreases with increasing thickness. Therefore, the nozzle heat transfer for tests with the cooled

inlet is less than the values corresponding to tests with the adiabatic inlet.

Heat transfer in a roughened nozzle. - The smooth nozzle was successively roughened three times and the resulting heat transfer was measured. One should start with station 4 (fig. 6), but since its heat transfer has not been significantly affected by acceleration, the results at station 8 (fig. 7) are analyzed first. For the first level of rough-

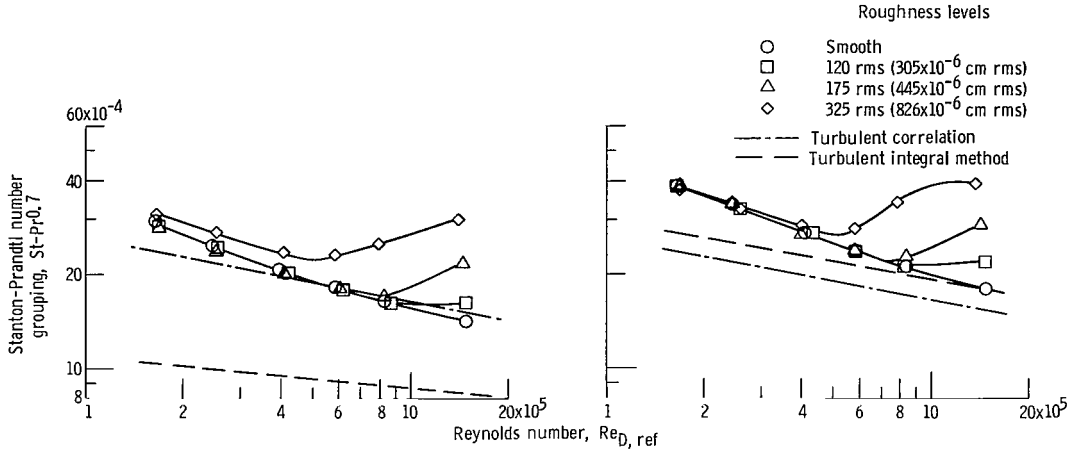

(a) Cooled inlet. (b) Adiabatic inlet.

Figure 6. - Experimental heat transfer for various degrees of roughness at station 4 (subsonic).

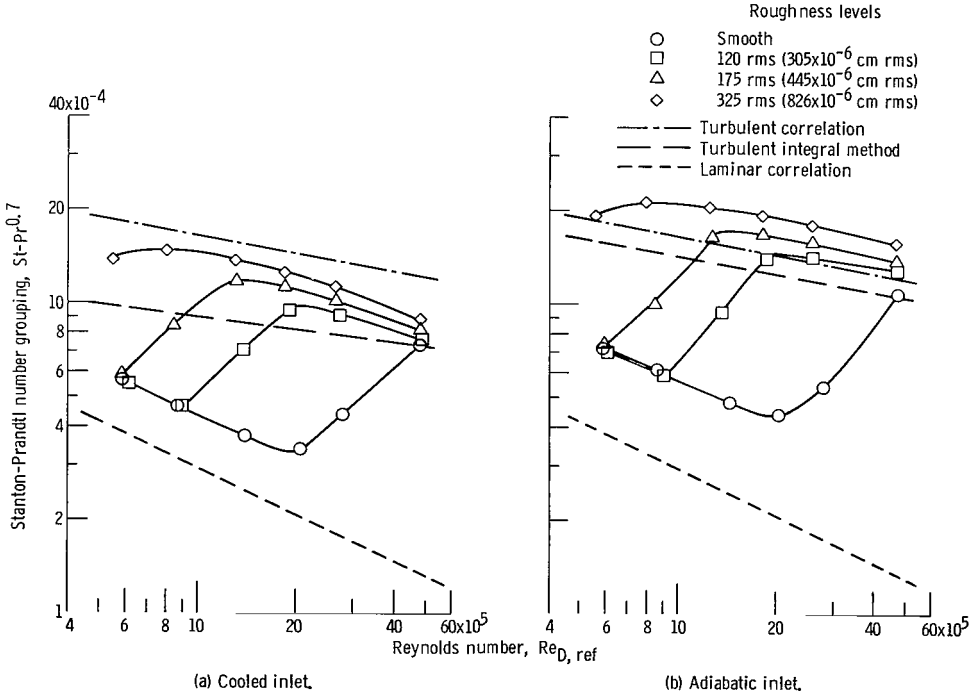

(a) Cooled inlet. (b) Adiabatic inlet.

Figure 7. - Experimental heat transfer for various degrees of roughness at station 8 (subsonic).

ness, 120 rms (305×10^{-6} cm rms), the heat-transfer parameter for the highest Reynolds number is about the same as it was for the smooth nozzle. However, this time as $Re_{D,ref}$ decreases, the heat transfer increases, then goes into transition, and at $Re_{D,ref} = 0.9\times10^{6}$ it increases again. At the second level of roughness, 175 rms (445×10^{-6} cm rms), the heat-transfer parameter increases and then takes a sharp drop for decreasing Reynolds number. At the highest roughness level, 325 rms (826×10^{-6} cm rms), figure 7 shows an increase in heat-transfer parameter and then the beginning of a sharp decrease. For the nozzle heat-transfer results shown in figure 7(a) the air passed through a water-cooled inlet before entering the nozzle. In the heat-transfer results of figure 7(b) the fluid thermal history prior to entering the nozzle is established by using an adiabatic inlet. The effect of operating with the cooled inlet in contrast to the adiabatic inlet is to decrease the value of $St\text{-}Pr^{0.7}$ at a given Reynolds number by a constant percentage. Moving downstream to the throat, the data in figure 8 show the same trends

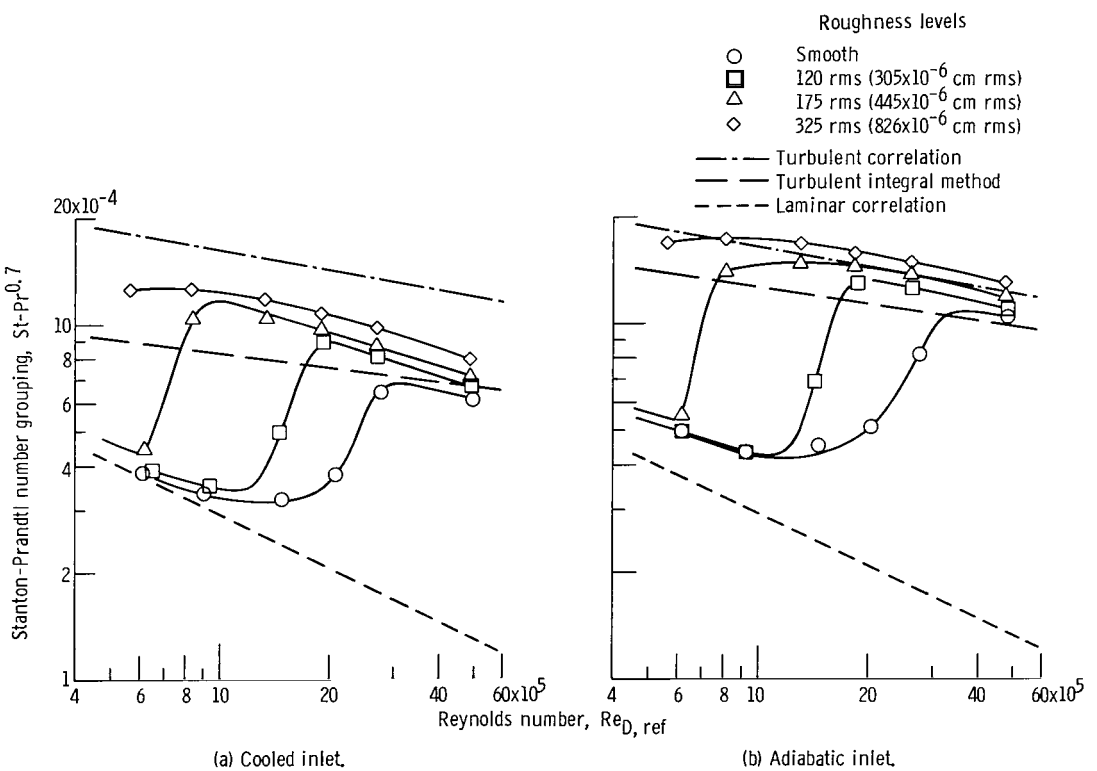

Figure 8. - Experimental heat transfer for various degrees of roughness at station 10 (throat).

as were seen in figure 7. At the highest Reynolds number all the experimental heat-transfer parameters are in the turbulent regime.

There is a certain amount of error in measuring the heat transfer in general, and

sandblasting of the nozzle walls may damage the heat meters. Therefore, a change in heat transfer of about 10 percent or less is inconclusive. At the first level of roughness the increase in heat transfer is negligible (<10 percent), at the second level it increases by 17 percent, and at the third the increase is 30 percent.

For the turbulent regime, according to reference 10, the effects of roughness become significant when the roughness height is equal to or greater than the sublayer height. When a u^+, y^+ model of the boundary layer profile in which the sublayer terminates at $y^+ \approx 20$ is used, estimates of the sublayer height can be obtained from the following relation:

$$y = \frac{y^+ D \frac{\mu_w}{\mu_\infty}}{\sqrt{\left(\frac{C_f}{2}\right)_{rough} \frac{t_\infty}{t_w} Re_D}}$$

The approximate value of $(C_f/2)_{rough}$ is found by getting a $(C_f/2)_{smooth}$ from reference 12 and then using the approximation

$$\left(\frac{C_f}{2}\right)_{rough} = \left(\frac{C_f}{2}\right)_{smooth} \frac{(St\text{-}Pr^{0.7})_{rough}}{(St\text{-}Pr^{0.7})_{smooth}}$$

For $Re_{D,\,ref} = 5\times10^6$ at the throat station, the estimated values of the sublayer heights are as follows:

Surface	Inlet			
	Adiabatic		Cooled	
	in.	cm	in.	cm
Smooth	0.190×10^{-3}	0.483×10^{-3}	0.201×10^{-3}	0.511×10^{-3}
120 rms (305×10^{-6} cm rms)	.184	.467	.191	.485
175 rms (445×10^{-6} cm rms)	.158	.401	.188	.478
325 rms (826×10^{-6} cm rms)	.152	.386	.184	.467

The experimental results of figure 8 are consistent with the hypothesis of Nikuradse (ref. 10). This hypothesis states that when the sublayer height is greater than the rough-

ness height heat transfer is not affected, but when it is in the region of or less than the roughness height heat transfer is affected. We must remember that Nikuradse's hypothesis only applies to the turbulent boundary layer. At the next decreasing Reynolds number the smooth wall heat transfer has gone into transition and the heat transfer on the rough walls has increased slightly, but the values in relation to each other remain the same. As $Re_{D, ref}$ is decreased further, the heat-transfer parameter corresponding to the first value of roughness goes into transition. With succeeding reductions in Reynolds number, the heat transfer corresponding to the second and third values of roughness, respectively, go into transition. At the low Reynolds numbers the smooth and the 120 rms (305×10^{-6} cm rms) wall are in the laminarization regime and their heat-transfer values are the same. In figure 8(b) the heat-transfer results for the adiabatic inlet are similar to those of the cooled inlet except that for a given Reynolds number the corresponding value of $St \cdot Pr^{0.7}$ is higher. For the turbulent regime the increase in heat transfer is 50 percent whereas an increase of 25 percent was observed in the laminarized regime.

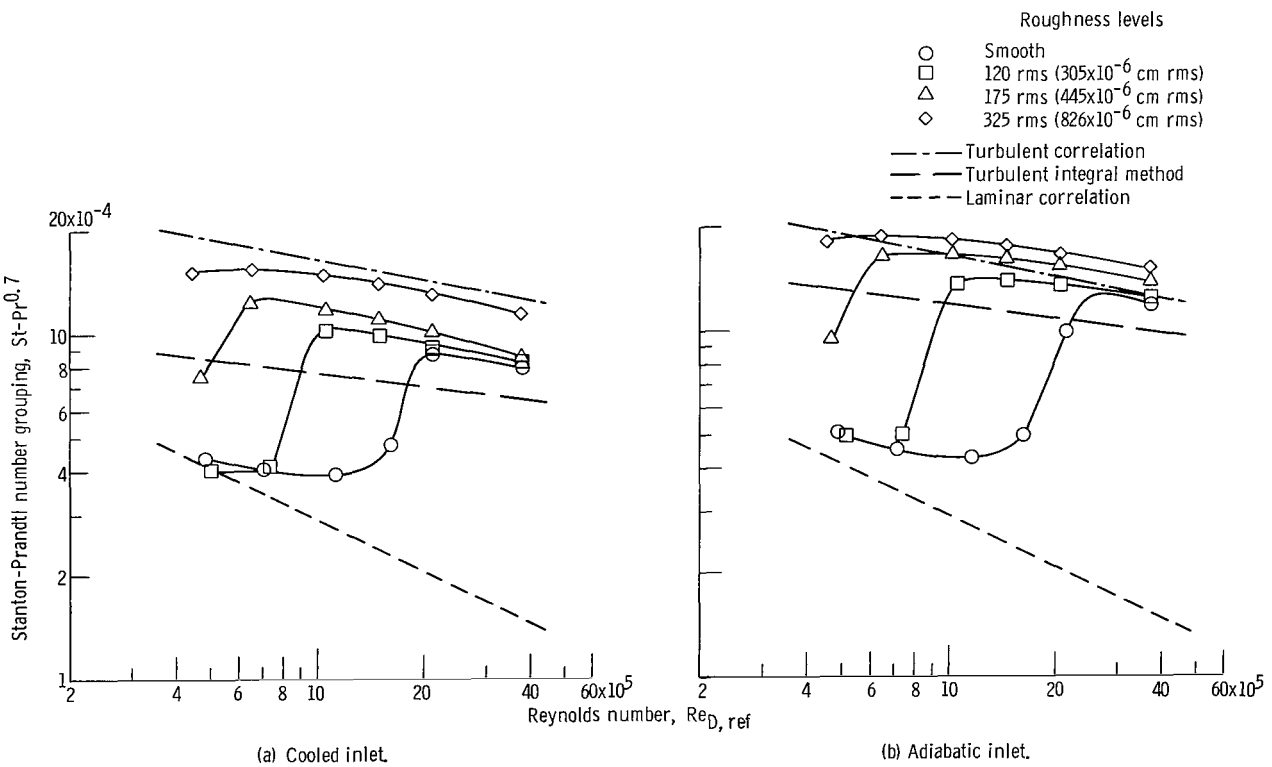

Figure 9. - Experimental heat transfer for various degrees of roughness at station 13 (supersonic).

The heat transfer at the supersonic station (fig. 9) behaves similarly to that of stations 8 and 10 except that there are more points in the turbulent heat-transfer regime

and less in the laminarization regime. This is due to the decrease in flow acceleration rate.

Returning to station 4 (fig. 6) we find the results difficult to explain. Since the heat-transfer parameter is turbulent for the smooth nozzle one would expect the effects of roughness to be similar to those of the turbulent heat-transfer regions of the other stations, and indeed they are for the three low Reynolds number points. However, at the high Reynolds number points, increased roughness appears to enhance the heat transfer drastically. It is possible that in the high Reynolds number region the sublayer height is very small and consequently the roughness height can be greater than the sublayer height. In contrast, at lower values of Re ($<5\times10^5$) the sublayer height can be greater than the roughness height where upon little effect of roughness on heat transfer will be observed. Unfortunately, this cannot be verified because the value for $(C_f/2)_{rough}$ in the sublayer approximation cannot be determined for station 4.

Moving downstream from station 4 the change in heat transfer with increasing axial distance is reviewed. At station 8, where the acceleration is a maximum, the heat-transfer mode is turbulent at the high Reynolds number and goes through transition to laminarization with the rough walls being able to maintain turbulent heat transfer for a wider Reynolds number range than the smooth. At station 10, as the flow acceleration decreases there are fewer points in the laminarization regime. And at station 13, in the supersonic region, as figure 9 shows, most of the laminarized values have gone into transition and those in transition have gone back to turbulent.

Fluid thermal history has the same effects on heat transfer at the other stations as it had at station 10.

The ratios of static to total pressure do not change noticeably with roughness. The small differences that do arise (<2 percent) are probably caused by sandblasting damage to the static pressure taps. The pressure ratios for all stations of the nozzle are given in table I.

TABLE I. - STATIC TO TOTAL PRESSURE RATIOS

Station	Area ratio, A/A_t	Pressure ratio, p_s/p_0	
		Experimental	One-dimensional
2	14.663	0.99996	0.99891
3	9.352	.99907	.99731
4	7.769	.99826	.99610
5	6.299	.99691	.99405
6	3.322	.9811	.97825
7	2.373	.9560	.95631
8	1.341	.8227	.84342
9	1.023	.5680	.62815
10	1.000	.4681	.52828
11	1.030	.3383	.41399
12	1.090	.2612	.33605
13	1.172	.2222	.27469
14	1.349	.1765	.19898
15	1.876	.1103	.10530

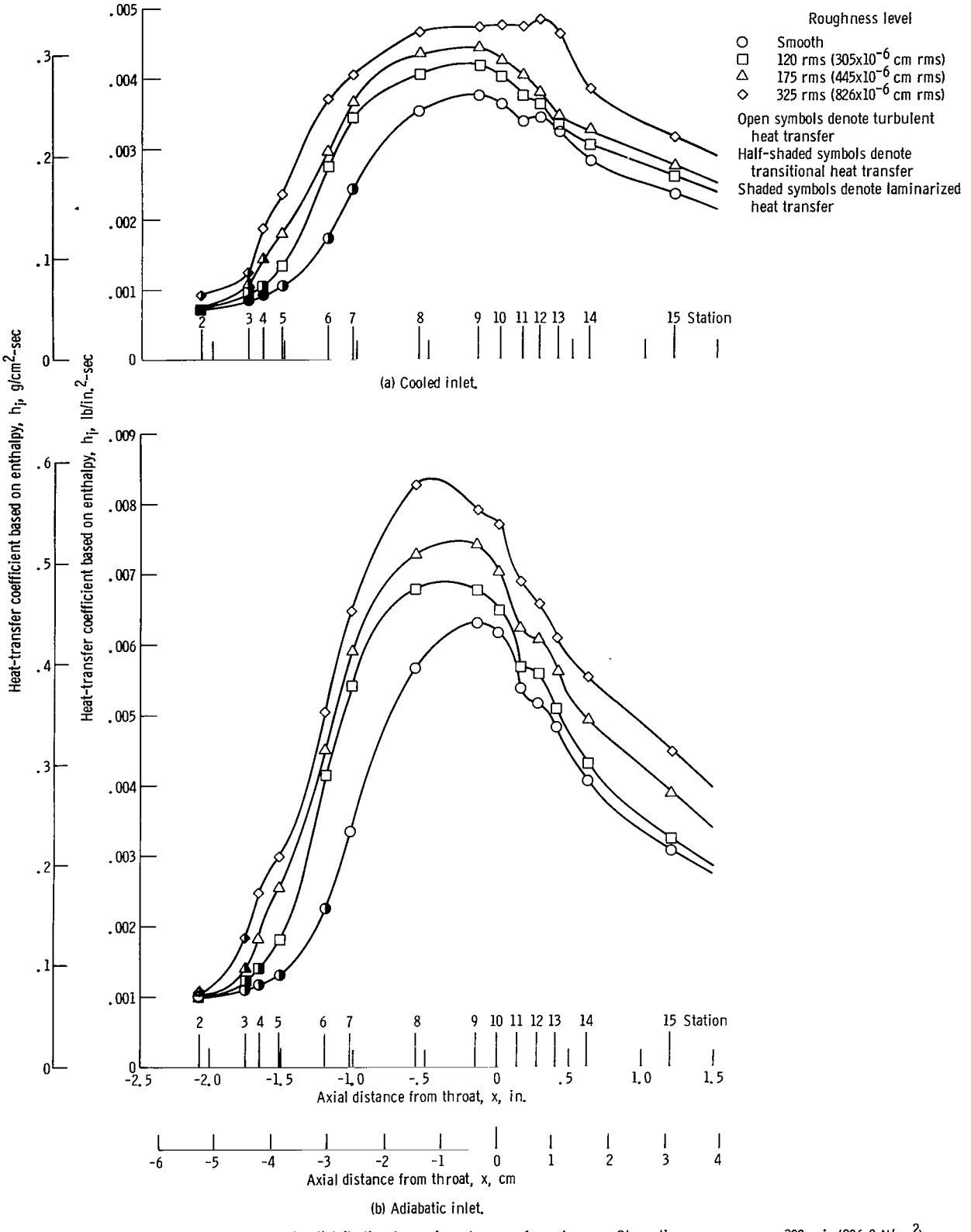

Figure 10. - Experimental heat-transfer distribution for various degrees of roughness. Stagnation pressure, p_0 = 300 psia (206.9 N/cm²).

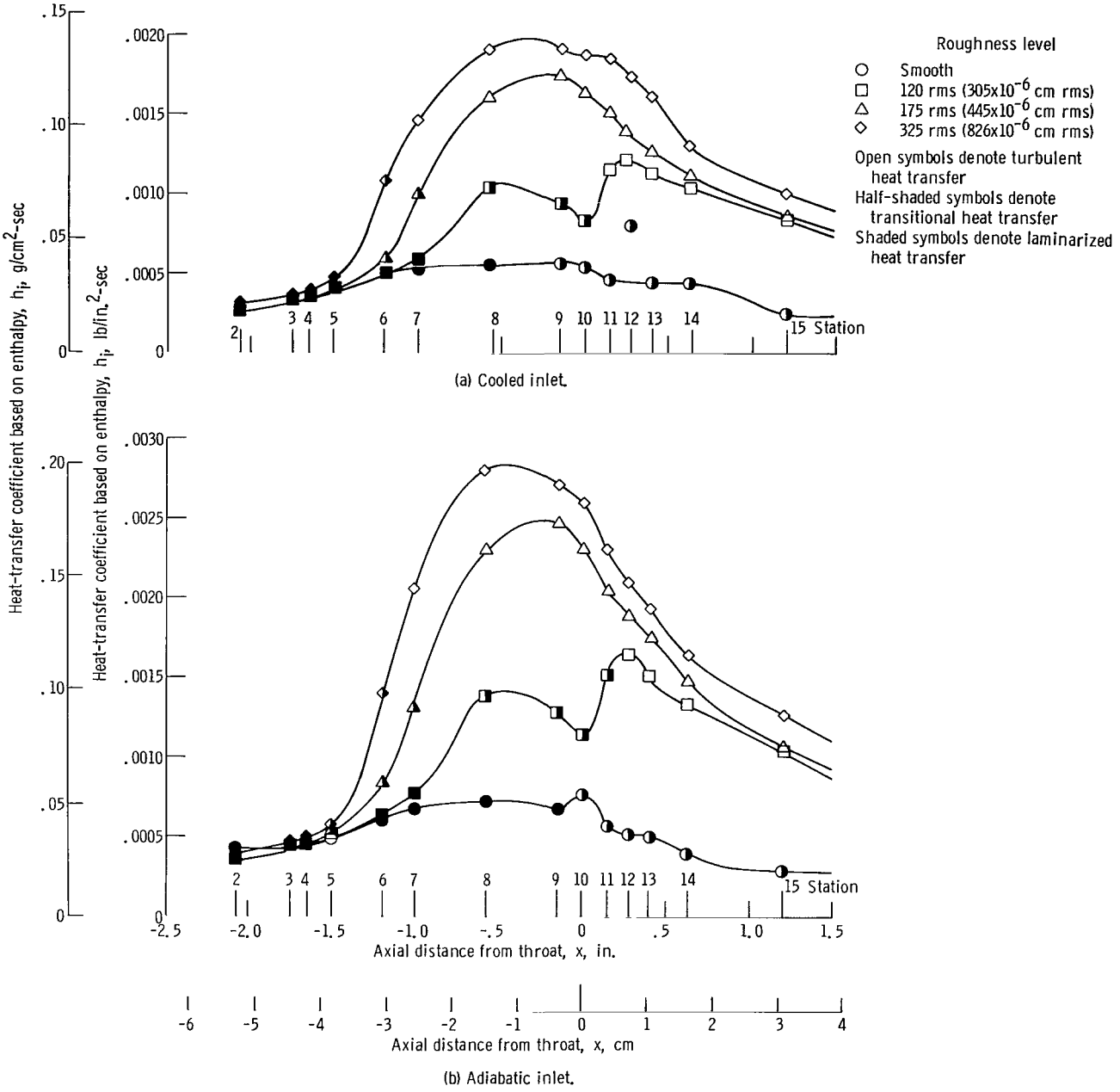

Figure 11. - Experimental heat-transfer distribution for various degrees of roughness. Stagnation pressure, p_0 = 75 psia (51.7 N/cm^2).

Axial Distribution of Heat-Transfer Coefficient

Figures 10 to 12 show the heat-transfer coefficient h_i as a function of axial distance from the nozzle throat. Some of the experimental values of heat-transfer coefficient h_i and wall temperature T_w are shown in tables II and III, respectively. Figure 10 shows

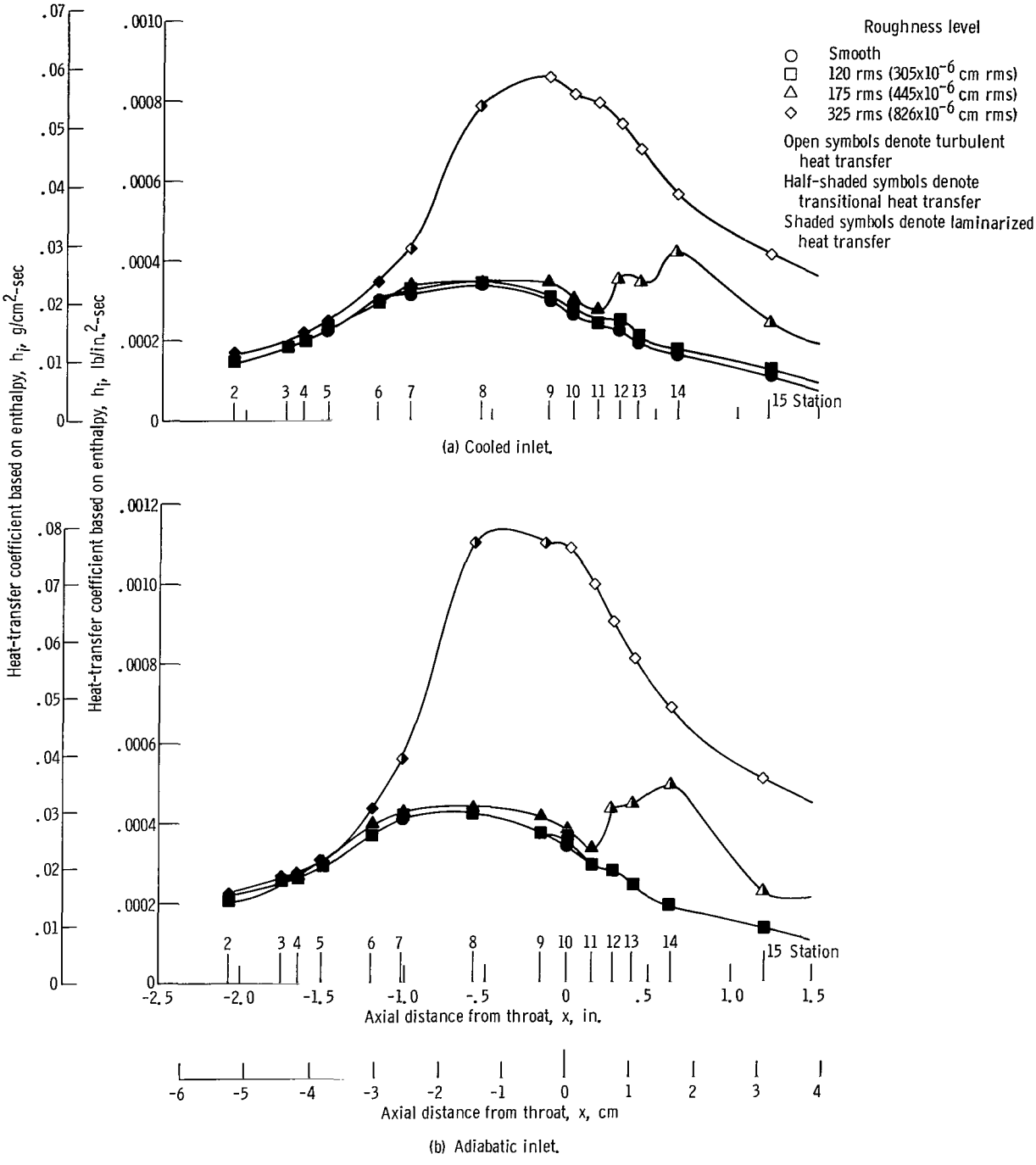

(a) Cooled inlet.

(b) Adiabatic inlet.

Figure 12. - Experimental heat-transfer distribution for various degrees of roughness. Stagnation pressure, p_0 = 30 psia (20.7 N/cm^2).

TABLE II. - EXPERIMENTAL HEAT-TRANSFER COEFFICIENTS

[Stagnation temperature, T_0, 970° R (539 K).]

(a) Cooled inlet

(a-1) U.S. Customary units

Station	Axial distance, x, in.	Diameter, D, in.	Stagnation pressure, p_0 = 300 psia				Stagnation pressure, p_0 = 75 psia				Stagnation pressure, p_0 = 30 psia			
			Nozzle roughness											
			Smooth	120 rms	175 rms	325 rms	Smooth	120 rms	175 rms	325 rms	Smooth	120 rms	175 rms	325 rms
			Heat-transfer coefficient based on enthalpy, h, lbm/(in.^{2})(sec)											
2	-2.085	5.740	0.712×10^{-3}	0.722×10^{-3}	0.715×10^{-3}	0.917×10^{-3}	0.265×10^{-3}	0.265×10^{-3}	0.255×10^{-3}	0.320×10^{-3}	0.145×10^{-3}	0.144×10^{-3}	0.138×10^{-3}	0.169×10^{-3}
3	-1.752	4.584	.831	.907	1.11	1.26	.325	.325	.326	.347	.181	.185	.183	.186
4	-1.635	4.178	.927	1.06	1.40	1.90	.347	.349	.346	.411	.201	.200	.193	.216
5	-1.515	3.762	1.06	1.36	1.80	2.37	.393	.385	.389	.474	.231	.223	.218	.247
6	-1.206	2.732	1.73	2.74	2.94	3.70	.501	.495	.589	1.07	.301	.288	.288	.350
7	-1.020	2.309	2.44	3.46	3.68	4.06	.527	.587	.988	1.45	.315	.326	.331	.433
8	-.581	1.736	3.56	4.07	4.35	4.69	.550	1.01	1.61	1.90	.331	.337	.347	.785
9	-.146	1.516	3.79	4.20	4.44	4.76	.563	.931	1.73	1.90	.299	.303	.344	.857
10	0	1.499	3.66	4.02	4.28	4.78	.537	.825	1.62	1.86	.261	.273	.303	.812
11	.150	1.521	3.40	3.79	4.07	4.75	.463	1.15	1.49	1.84	.239	.237	.272	.796
12	.277	1.565	3.48	3.66	3.80	4.88	.801	1.22	1.38	1.72	.247	.219	.352	.738
13	.400	1.623	3.25	3.33	3.47	4.62	.445	1.12	1.26	1.59	.204	.193	.346	.676
14	.622	1.741	2.87	3.06	3.26	3.82	.436	1.04	1.12	1.30	.177	.162	.423	.563
15	1.209	2.053	2.38	2.60	2.77	3.15	.251	.834	.850	1.00	.120	.109	.241	.418

(a-2) SI Units

Station	Axial distance, x, cm	Diameter, D, cm	Stagnation pressure, p_0 = 206.9 N/cm^2				Stagnation pressure, p_0 = 51.7 N/cm^2				Stagnation pressure, p_0 = 20.7 N/cm^2			
			Nozzle roughness											
			Smooth	305×10^{-6} cm rms	445×10^{-6} cm rms	826×10^{-6} cm rms	Smooth	305×10^{-6} cm rms	445×10^{-6} cm rms	826×10^{-6} cm rms	Smooth	305×10^{-6} cm rms	445×10^{-6} cm rms	826×10^{-6} cm rms
			Heat-transfer coefficient based on enthalpy, h, g/(cm^2)(sec)											
2	-5.296	14.580	0.0498	0.0505	0.0500	0.0641	0.0185	0.0185	0.0178	0.0224	0.0101	0.0101	0.00965	0.0118
3	-4.450	11.643	.0581	.0634	.0776	.0881	.0227	.0227	.0228	.0243	.0127	.0129	.0128	.0130
4	-4.153	10.612	.0648	.0741	.0979	.1328	.0243	.0244	.0242	.0287	.0140	.0140	.0135	.0151
5	-3.848	9.555	.0741	.0951	.1258	.1657	.0275	.0269	.0272	.0331	.0161	.0156	.0152	.0173
6	-3.063	6.939	.1209	.1915	.2055	.2586	.0350	.0346	.0412	.0248	.0210	.0201	.0201	.0245
7	-2.591	5.865	.1706	.2419	.2572	.2838	.0368	.0410	.0691	.1014	.0220	.0228	.0231	.0303
8	-1.476	4.409	.2488	.2845	.3041	.3278	.0384	.0706	.1125	.1328	.0231	.0236	.0243	.0549
9	-.371	3.851	.2649	.2936	.3104	.3327	.0394	.0651	.1209	.1328	.0209	.0212	.0240	.0599
10	0	3.807	.2558	.2810	.2992	.3341	.0375	.0577	.1132	.1300	.0182	.0191	.0212	.0568
11	.381	3.863	.2377	.2649	.2845	.3320	.0324	.0804	.1042	.1286	.0167	.0166	.0190	.0556
12	.704	3.975	.2433	.2558	.2656	.3411	.0560	.0853	.0965	.1202	.0173	.0153	.0246	.0516
13	1.016	4.122	.2272	.2328	.2426	.3229	.0311	.0783	.0881	.1111	.0143	.0135	.0242	.0473
14	1.580	4.422	.2006	.2139	.2279	.2670	.0305	.0727	.0783	.0909	.0124	.0113	.0296	.0394
15	3.071	5.215	.1664	.1817	.1936	.2202	.0175	.0583	.0594	.0699	.00839	.00762	.0168	.0292

TABLE II. - Concluded. EXPERIMENTAL HEAT-TRANSFER COEFFICIENTS

(b) Adiabatic inlet

(b-1) U.S. Customary Units

Station	Axial distance, x, in.	Diameter, D, in.	Stagnation pressure, p_0 = 300 psia				Stagnation pressure, p_0 = 75 psia				Stagnation pressure, p_0 = 30 psia			
			Nozzle roughness											
			Smooth	120 rms	175 rms	325 rms	Smooth	120 rms	175 rms	325 rms	Smooth	120 rms	175 rms	325 rms
			Heat-transfer coefficient based on enthalpy, h, lbm/(in.^{2})(sec)											
2	-2.085	5.740	1.03×10^{-3}	0.988×10^{-3}	0.985×10^{-3}	1.05×10^{-3}	0.417×10^{-3}	0.379×10^{-3}	0.366×10^{-3}	0.358×10^{-3}	0.227×10^{-3}	0.213×10^{-3}	0.202×10^{-3}	0.204×10^{-3}
3	-1.752	4.584	1.12	1.24	1.41	1.83	.449	.444	.450	.456	.259	.258	.265	.251
4	-1.635	4.178	1.18	1.41	1.84	2.49	.460	.461	.465	.490	.266	.270	.269	.264
5	-1.515	3.762	1.30	1.79	2.57	2.98	.486	.490	.518	.563	.283	.290	.302	.296
6	-1.206	2.732	2.25	4.12	4.51	5.03	.617	.644	.821	1.40	.369	.381	.398	.432
7	-1.020	2.309	3.35	5.38	5.90	6.47	.673	.759	1.30	2.06	.399	.409	.416	.564
8	-.581	1.736	5.67	6.77	7.25	8.27	.719	1.36	2.29	2.81	.424	.425	.436	1.10
9	-.146	1.516	6.30	6.76	7.39	7.89	.674	1.27	2.47	2.70	.373	.376	.416	1.11
10	0	1.499	6.15	6.48	7.03	7.72	.758	1.15	2.29	2.60	.340	.349	.385	1.09
11	.150	1.521	5.37	5.68	6.24	6.89	.576	1.53	2.04	2.32	.298	.297	.334	1.01
12	.277	1.565	5.16	5.60	6.07	6.55	.526	1.66	1.89	2.10	.475	.281	.435	.906
13	.400	1.623	4.83	5.08	5.61	6.07	.506	1.50	1.76	1.94	.241	.244	.444	.815
14	.622	1.741	4.08	4.29	4.92	5.44	.396	1.33	1.47	1.64	.201	.192	.497	.689
15	1.209	2.053	3.06	3.25	3.90	4.45	.298	1.04	1.08	1.27	.130	.138	.223	.510

(b-2) SI Units

Station	Axial distance, x, cm	Diameter, D, cm	Stagnation pressure, p_0 = 206.9 N/cm^2				Stagnation pressure, p_0 = 51.7 N/cm^2				Stagnation pressure, p_0 = 20.7 N/cm^2			
			Nozzle roughness											
			Smooth	305×10^{-6} cm rms	445×10^{-6} cm rms	826×10^{-6} cm rms	Smooth	305×10^{-6} cm rms	445×10^{-6} cm rms	826×10^{-6} cm rms	Smooth	305×10^{-6} cm rms	445×10^{-6} cm rms	626×10^{-6} cm rms
			Heat-transfer coefficient based on enthalpy, h, g/(cm^2)(sec)											
2	-5.296	14.580	0.0720	0.0691	0.0689	0.0734	0.0291	0.0265	0.0256	0.0250	0.0159	0.0149	0.0141	0.0143
3	-4.450	11.643	.0783	.0867	.0986	.1279	.0314	.0310	.0315	.0319	.0181	.0180	.0185	.0175
4	-4.153	10.612	.0825	.0986	.1286	.1741	.0322	.0322	.0325	.0343	.0186	.0189	.0188	.0185
5	-3.848	9.555	.0909	.1251	.1796	.2083	.0340	.0343	.0362	.0394	.0198	.0203	.0211	.0207
6	-3.063	6.939	.1573	.2880	.3152	.3516	.0431	.0450	.0574	.0979	.0258	.0266	.0278	.0302
7	-2.591	5.865	.2342	.3761	.4124	.4523	.0470	.0531	.0909	.1440	.0279	.0286	.0291	.0394
8	-1.476	4.409	.3963	.4732	.5068	.5781	.0503	.0951	.1601	.1964	.0296	.0297	.0305	.0769
9	-.371	3.851	.4404	.4725	.5166	.5515	.0471	.0888	.1727	.1887	.0261	.0263	.0291	.0776
10	0	3.807	.4299	.4530	.4914	.5396	.0530	.0804	.1601	.1817	.0238	.0244	.0269	.0762
11	.381	3.863	.3754	.3970	.4362	.4816	.0403	.1069	.1426	.1622	.0208	.0208	.0233	.0706
12	.704	3.975	.3607	.3914	.4243	.4578	.0368	.1160	.1321	.1468	.0332	.0196	.0304	.0633
13	1.016	4.122	.3376	.3551	.3921	.4243	.0354	.1048	.1230	.1356	.0168	.0171	.0310	.0570
14	1.580	4.422	.2852	.2999	.3439	.3803	.0277	.0930	.1028	.1146	.0140	.0134	.0347	.0482
15	3.071	5.215	.2139	.2272	.2726	.3111	.0208	.0727	.0755	.0888	.00909	.00965	.0156	.0356

TABLE III. - Concluded. EXPERIMENTAL WALL TEMPERATURES

(b) Adiabatic inlet

(b-1) U.S. Customary Units

Station	Axial distance, x, in.	Diameter, D, in.	Stagnation pressure, p_0 = 300 psia				Stagnation pressure, p_0 = 75 psia				Stagnation pressure, p_0 = 30 psia			
			Nozzle roughness											
			Smooth	120 rms	175 rms	325 rms	Smooth	120 rms	175 rms	325 rms	Smooth	120 rms	175 rms	325 rms
			Wall temperature, T_w, ^oR											
2	-2.085	5.740	718.1	689.1	711.1	718.3	634.0	598.3	617.9	620.1	594.7	560.2	581.1	587.1
3	-1.752	4.584	719.7	710.5	744.5	770.5	633.3	607.7	630.4	634.4	596.8	568.9	591.7	595.0
4	-1.635	4.178	726.1	723.4	771.0	800.4	636.5	609.5	632.1	638.9	599.5	570.8	592.5	597.8
5	-1.515	3.762	735.2	751.3	802.4	818.4	640.2	615.8	639.4	650.8	602.8	575.8	598.5	604.4
6	-1.206	2.732	792.2	839.4	858.7	866.6	659.7	642.4	686.2	741.8	618.7	595.0	619.1	631.2
7	-1.020	2.309	833.9	863.6	879.3	885.3	671.1	660.2	735.7	783.8	627.5	601.7	625.1	654.2
8	-.581	1.736	872.2	876.3	890.5	896.6	675.3	719.7	793.4	811.9	629.9	603.8	628.7	713.8
9	-.146	1.516	871.4	867.6	881.6	884.7	665.6	708.3	792.2	800.2	617.9	591.3	619.3	710.8
10	0	1.499	865.3	861.3	875.4	879.5	674.1	694.6	783.5	794.0	610.4	585.2	614.1	706.2
11	.150	1.521	852.9	847.7	863.6	868.1	652.3	724.7	770.5	781.0	603.7	575.4	605.5	697.7
12	.277	1.565	842.8	838.2	853.6	857.2	640.4	725.6	755.4	764.4	611.4	568.5	619.4	682.6
13	.400	1.623	834.2	829.3	847.5	851.2	636.7	714.9	747.4	755.8	589.8	561.3	621.6	672.8
14	.622	1.741	817.6	811.0	832.0	838.6	617.7	697.3	723.7	735.3	580.6	547.1	624.9	655.1
15	1.209	2.053	792.1	781.8	806.6	816.4	598.5	664.9	688.3	704.8	564.5	530.3	574.6	627.8

(b-2) SI Units

Station	Axial distance, x, cm	Diameter, D, cm	Stagnation pressure, p_0 = 206.9 N/cm^2				Stagnation pressure, p_0 = 51.7 N/cm^2				Stagnation pressure, p_0 = 20.7 N/cm^2			
			Nozzle roughness											
			Smooth	305×10^{-6} cm rms	445×10^{-6} cm rms	826×10^{-6} cm rms	Smooth	305×10^{-6} cm rms	445×10^{-6} cm rms	826×10^{-6} cm rms	Smooth	305×10^{-6} cm rms	445×10^{-6} cm rms	826×10^{-6} cm rms
			Wall temperature, T_w, K											
2	-5.296	14.580	398.9	382.8	395.1	399.1	352.2	332.4	343.3	344.5	330.4	311.2	322.8	326.2
3	-4.450	11.643	399.8	394.7	413.6	428.1	351.8	337.6	350.2	352.4	331.6	316.1	328.7	330.6
4	-4.153	10.612	403.4	401.9	428.3	444.7	353.6	338.6	351.2	354.9	333.1	317.1	329.2	332.1
5	-3.848	9.555	408.4	417.4	445.8	454.7	355.7	342.1	355.2	361.6	334.9	319.9	332.5	335.8
6	-3.063	6.939	440.1	466.3	477.1	481.4	366.5	356.9	381.2	412.1	343.7	330.6	343.9	350.7
7	-2.591	5.865	463.3	479.8	488.5	491.8	372.8	366.8	408.7	435.4	348.6	334.3	347.3	363.4
8	-1.476	4.409	484.6	486.8	494.7	498.1	375.2	399.8	440.8	451.1	349.9	335.4	349.3	396.6
9	-.371	3.851	484.1	482.0	489.8	491.5	369.8	393.5	440.1	444.6	343.3	328.5	344.1	394.9
10	0	3.807	480.7	478.5	486.3	488.6	374.5	385.9	435.3	441.1	339.1	325.1	341.2	392.3
11	.381	3.863	473.8	470.9	479.8	482.3	362.4	402.6	428.1	433.9	335.4	319.7	336.4	387.6
12	.704	3.975	468.2	465.7	474.2	476.2	355.8	403.1	419.7	424.7	339.7	315.8	344.1	379.2
13	1.016	4.122	463.4	460.7	470.8	472.9	353.7	397.2	415.2	419.9	327.7	311.8	345.3	373.8
14	1.580	4.422	454.2	450.6	462.2	465.9	343.2	387.4	402.1	408.5	322.6	303.9	347.2	363.9
15	3.071	5.215	440.1	434.3	448.1	453.6	332.5	369.4	382.4	391.6	313.6	294.6	319.2	348.8

TABLE III. - EXPERIMENTAL WALL TEMPERATURES

[Stagnation temperature, T_0, 970° R (539 K).]

(a) Cooled inlet

(a-1) U.S. Customary Units

Station	Axial distance, x, in.	Diameter, D, in.	Stagnation pressure, p_0 = 300 psia				Stagnation pressure, p_0 = 75 psia				Stagnation pressure, p_0 = 30 psia			
			Nozzle roughness											
			Smooth	120 rms	175 rms	325 rms	Smooth	120 rms	175 rms	325 rms	Smooth	120 rms	175 rms	325 rms
			Wall temperature, T_w, °R											
2	-2.085	5.740	699.8	680.2	691.9	719.0	616.5	590.5	603.5	623.9	584.2	555.3	570.1	586.9
3	-1.752	4.584	713.4	704.2	732.6	745.0	627.2	601.3	616.4	627.5	593.1	564.1	579.5	590.8
4	-1.635	4.178	720.6	714.7	751.1	790.6	630.7	602.8	618.2	639.3	596.0	566.0	581.0	596.0
5	-1.515	3.762	731.4	739.7	776.7	806.6	637.6	610.4	625.5	649.2	602.3	571.5	586.3	602.4
6	-1.206	2.732	781.4	817.7	827.9	846.9	656.2	637.9	670.4	723.5	617.9	590.8	606.4	625.5
7	-1.020	2.309	817.6	836.2	843.4	855.9	664.4	648.0	709.0	754.1	625.4	594.6	610.5	638.9
8	-.581	1.736	847.9	850.0	856.7	865.2	667.6	702.9	760.2	781.0	627.1	599.4	616.2	688.2
9	-.146	1.516	845.2	843.9	851.4	856.2	663.9	691.5	761.7	774.0	615.4	589.0	612.4	692.2
10	0	1.499	841.8	839.5	846.7	853.6	665.5	678.7	754.1	771.2	611.4	583.2	604.4	689.1
11	.150	1.521	829.9	827.9	835.3	853.6	654.1	708.2	740.2	766.0	605.6	574.0	606.7	684.1
12	.277	1.565	824.3	819.3	825.3	843.9	690.1	711.7	730.7	753.0	603.4	570.0	611.3	673.2
13	.400	1.623	817.0	810.9	818.3	836.1	645.7	703.1	723.4	743.5	596.1	564.2	612.5	664.6
14	.622	1.741	801.1	794.8	803.6	817.6	635.8	685.1	701.4	720.0	585.7	550.5	616.9	645.4
15	1.209	2.053	777.3	775.3	785.5	797.9	600.8	662.0	675.2	694.2	569.6	536.8	585.0	623.1

(a-2) SI Units

Station	Axial distance, x, cm	Diameter, D, cm	Stagnation pressure, p_0 = 206.9 N/cm^2				Stagnation pressure, p_0 = 51.7 N/cm^2				Stagnation pressure, p_0 = 20.7 N/cm^2			
			Nozzle roughness											
			Smooth	305×10^{-6} cm rms	445×10^{-6} cm rms	826×10^{-6} cm rms	Smooth	305×10^{-6} cm rms	445×10^{-6} cm rms	826×10^{-6} cm rms	Smooth	305×10^{-6} cm rms	445×10^{-6} cm rms	826×10^{-6} cm rms
			Wall temperature, T_w, K											
2	-5.296	14.580	388.8	377.9	384.4	399.4	342.5	328.1	335.3	346.6	324.6	308.5	316.7	326.1
3	-4.450	11.643	396.3	391.2	407.0	413.9	348.4	334.1	342.4	348.6	329.5	313.4	321.9	328.2
4	-4.153	10.612	400.3	397.1	417.3	439.2	350.4	334.9	343.4	355.2	331.1	314.4	322.8	331.1
5	-3.848	9.555	406.3	410.9	431.5	448.1	354.2	339.1	347.5	360.7	334.6	317.5	325.7	334.7
6	-3.063	6.939	434.1	454.3	459.9	470.5	364.6	354.4	372.4	401.9	343.3	328.2	336.9	347.5
7	-2.591	5.865	454.2	464.6	468.6	475.5	369.1	360.0	393.9	418.9	347.4	330.3	339.2	354.9
8	-1.476	4.409	471.1	472.2	475.9	480.7	370.9	390.5	422.3	433.9	348.4	333.0	342.3	382.3
9	-.371	3.851	469.6	468.8	473.0	475.7	368.8	384.2	423.2	430.0	341.9	327.2	340.2	384.6
10	0	3.807	467.7	466.4	470.4	474.2	369.7	377.1	418.9	428.4	339.7	324.0	335.8	382.8
11	.381	3.863	461.1	459.9	464.1	474.2	363.4	393.4	411.2	425.6	336.4	318.9	337.1	380.1
12	.704	3.975	457.9	455.2	458.5	468.8	383.4	395.4	405.9	418.3	335.2	316.7	339.6	374.0
13	1.016	4.122	453.9	450.5	454.6	464.5	358.7	390.6	401.9	413.1	331.2	313.4	340.3	369.2
14	1.580	4.422	445.1	441.6	446.4	454.2	353.2	380.6	389.7	400.0	325.4	305.8	342.7	358.6
15	3.071	5.215	431.8	430.7	436.4	443.3	333.8	367.8	375.1	385.7	316.4	298.2	325.0	346.2

the heat-transfer coefficient for all values of roughness at a stagnation pressure p_0 of 300 psia (206.9 N/cm^2). The heat-transfer coefficient reaches a maximum in the vicinity of the throat and then decreases as the flow goes supersonic. The large differences in heat transfer between the smooth and the 120 rms (305×10^{-6} cm rms) wall at stations 6 and 7 occur because the smooth values are in transition while the 120 rms (305×10^{-6} cm rms) values are in the turbulent heat-transfer region. For a stagnation pressure, p_0 = 75 psia (51.7 N/cm^2), figure 11 shows that the heat transfer for the smooth wall is much less than that for the 175 and 325 rms (445×10^{-6} and 826×10^{-6} cm rms) walls. The heat transfer of the smooth wall is in the laminarization or lower transition regime while the heat transfer for the two rough walls are turbulent. The heat transfer at the 120 rms (305×10^{-6} cm rms) wall poses a very interesting situation because it reaches a maximum downstream of the throat. The heat transfer remains laminarized up to 1 inch (2.54 cm) upstream of the throat after which it goes into transition. It reaches a local maximum, then decreases, and just downstream of the throat makes a sudden jump into the turbulent regime to a peak value. This same phenomenon was observed in reference 4 where the investigator used a smooth nozzle wall and varied the total stagnation pressure. In both cases the sharp increase in heat transfer occurred where the nozzle exit cone meets the throat radius of curvature, and this change in geometry causes a slight adverse pressure gradient. If the heat transfer is originally in the transition region, the adverse gradient elevates it into the turbulent region. Figure 12 shows a similar phenomenon for a stagnation pressure of 30 psia (20.7 N/cm^2). Here, however, the heat transfer at the 120 rms (305×10^{-6} cm rms) wall remains laminarized while the 175 rms (445×10^{-6} cm rms) wall experiences the heat-transfer elevation.

Differences Between Present Experiment and Pipe Flow Studies

Unfortunately a direct comparison of the heat-transfer results of this report with those for rough pipes (refs. 7 to 9) cannot be made because of certain differences in the experiments. These differences encompass both the roughness height and Reynolds number range over which the experiments were conducted.

The roughness heights used in the nozzle are much smaller than those used in the pipes. The ratio of roughness height to nozzle diameter can be expressed as the roughness ratio e/D. For the largest value of nozzle roughness, 325 rms (826×10^{-6} cm rms), e/D = 0.00022 for a maximum value at the throat and e/D = 0.00006 for a minimum value at the nozzle entrance. For the lower values of nozzle roughness these ratios are proportionately smaller. The lowest of the roughness ratios used for pipes is found in reference 8 and is e/D = 0.00156, higher by a factor of 8 from the largest nozzle roughness ratio.

The Reynolds number for the nozzles ranged from about 6×10^5 to 5×10^6. However, in the pipe flow experiments of references 7 to 9, the maximum Reynolds number was only about 6×10^4. Although these large differences in Reynolds numbers coupled with the differences in roughness height preclude a comparison of nozzle and pipe flow results, the current study suggests that the assumption of Nikuradse (ref. 10), might be applicable to nozzle flows. This assumption is that the turbulent heat transfer is unaffected by roughness when the sublayer height is greater than the roughness height.

SUMMARY OF RESULTS

An experimental investigation has been performed to study the effects of various degrees of surface roughness on heat transfer in a converging-diverging nozzle. A summary of the results for a roughness range from smooth to 325 rms (826×10^{-6} cm rms) are as follows:

1. Roughness causes transition from laminarized flow to take place at a lower Reynolds number than that for a smooth wall.

2. In the laminarization regime, heat transfer is unaffected by roughness.

3. In the turbulent regime, the heat transfer is not noticeably affected until the roughness height is in the region of or greater than the approximated sublayer height.

4. Thermal history of the fluid before it enters the nozzle affects the heat transfer. An adiabatic inlet causes higher heat transfer than a cooled inlet for all values of roughness.

5. The pressure distribution is not noticeably affected by roughness.

Lewis Research Center,
National Aeronautics and Space Administration,
Cleveland, Ohio, April 23, 1970,
129-01.

REFERENCES

1. Boldman, D. R.; Schmidt, J. F.; and Ehlers, R. C.: Effect of Uncooled Inlet Length and Nozzle Convergence Angle on the Turbulent Boundary Layer and Heat Transfer in Conical Nozzles Operating with Air. J. Heat Transfer, vol. 89, no. 4, Nov. 1967, pp. 341-350.

2. Boldman, Donald R.; Neumann, Harvey E.; and Schmidt, James F.: Heat Transfer in 30° and 60° Half-Angle of Convergence Nozzles with Various Diameter Uncooled Pipe Inlets. NASA TN D-4177, 1967.

3. Graham, Robert W.; and Boldman, Donald R.: The Use of Energy Thickness in Prediction of Throat Heat Transfer in Rocket Nozzles. NASA TN D-5356, 1969.

4. Back, L. H.; Massier, P. F.; and Cuffel, R. F.: Flow Phenomena and Convective Heat Transfer in a Conical Supersonic Nozzle. J. Spacecraft Rockets, vol. 4, no. 8, Aug. 1967, pp. 1040-1047.

5. Boldman, Donald R.; Schmidt, James F.; and Gallagher, Anne K.: Laminarization of a Turbulent Boundary Layer as Observed from Heat-Transfer and Boundary-Layer Measurements in Conical Nozzles. NASA TN D-4788, 1968.

6. Cope, W. F.: The Friction and Heat-Transmission Coefficients of Rough Pipes. Proc. Inst. Mech. Eng., vol. 145, 1941, pp. 99-105.

7. Sams, Eldon W.: Experimental Investigation of Average Heat-Transfer and Friction Coefficients for Air Flowing in Circular Tubes Having Square-Thread-Type Roughness. NACA RM E52D17, 1952.

8. Smith, J. W.; and Epstein, Norman: Effect of Wall Roughness on Convective Heat Transfer in Commercial Pipes. AIChE J., vol. 3, no. 2, June 1957, pp. 242-248.

9. Nunner, Wolfgang (F. Hudswell, trans.): Heat Transfer and Pressure Drop in Rough Tubes. Rep. AERE-Lib/Trans-786, United Kingdom Atomic Energy Authority, 1958.

10. Nikuradse, J.: Laws of Flow in Rough Pipes. NACA TM 1292, 1950.

11. Beckwith, Ivan E.; and Gallagher, James J.: Heat Transfer and Recovery Temperatures on a Sphere with Laminar, Transitional, and Turbulent Boundary Layers at Mach Numbers of 2.00 and 4.15. NACA TN 4125, 1957.

12. Elliot, David G.; Bartz, Donald R.; and Silver, Sidney: Calculation of Turbulent Boundary-Layer Growth and Heat Transfer in Axi-Symmetric Nozzles. Tech. Rep. 32-387, Jet Propulsion Lab., California Inst. Tech., Feb. 15, 1963.

NASA-Langley, 1970 —— 12 E-5597

"The aeronautical and space activities of the United States shall be conducted so as to contribute . . . to the expansion of human knowledge of phenomena in the atmosphere and space. The Administration shall provide for the widest practicable and appropriate dissemination of information concerning its activities and the results thereof."

— NATIONAL AERONAUTICS AND SPACE ACT OF 1958

NASA SCIENTIFIC AND TECHNICAL PUBLICATIONS

TECHNICAL REPORTS: Scientific and technical information considered important, complete, and a lasting contribution to existing knowledge.

TECHNICAL NOTES: Information less broad in scope but nevertheless of importance as a contribution to existing knowledge.

TECHNICAL MEMORANDUMS: Information receiving limited distribution because of preliminary data, security classification, or other reasons.

CONTRACTOR REPORTS: Scientific and technical information generated under a NASA contract or grant and considered an important contribution to existing knowledge.

TECHNICAL TRANSLATIONS: Information published in a foreign language considered to merit NASA distribution in English.

SPECIAL PUBLICATIONS: Information derived from or of value to NASA activities. Publications include conference proceedings, monographs, data compilations, handbooks, sourcebooks, and special bibliographies.

TECHNOLOGY UTILIZATION PUBLICATIONS: Information on technology used by NASA that may be of particular interest in commercial and other non-aerospace applications. Publications include Tech Briefs, Technology Utilization Reports and Notes, and Technology Surveys.

Details on the availability of these publications may be obtained from:

SCIENTIFIC AND TECHNICAL INFORMATION DIVISION

NATIONAL AERONAUTICS AND SPACE ADMINISTRATION

Washington, D.C. 20546